Linear perylenetetracarboxylic monoanhydried derivatives for the sensitization of dye-sensitized solar cells

Guiju Qi[a], Renjie Li[b], Limin Wang[a], Xiyou Li[a,*]

[a] Key Lab of Colloid and Interface Chemistry, Ministry of Education, Department of Chemistry, Shandong University, 250100, China
[b] Department of Chemistry, Wuhan University, 430072, China

ARTICLE INFO

ABSTRACT

We report here a series of linear perylenetetracarboxylic imide derivatives (PDIs), abbreviated as PN, PO–PN and PO–PO–PN, with high molar extinction coefficients and broad absorptions in visible to near-infrared (NIR) region. These new dyes are designed for the use as sensitizers in dye sensitized solar cell (DSSC) with a motive to enhance the optical absorption of mesoporous titania film and light collecting efficiency. Energy transfer from PO parts to PN unit is revealed by absorption and fluorescence spectra. The energy transfer efficiencies estimated from the fluorescence quenching efficiencies are almost 100%. The mesoporous titania film loaded with these dyes exhibit broad absorption bands in the visible to NIR region. The IPCE spectra revealed distinctively the contribution of PO parts to the solar energy conversion, which suggests that the intramolecular singlet–singlet energy transfer is a reliable strategy to improve the light absorbing abilities of a dye adsorbed on titania films. The necessary efforts to further improve the efficiency of cells by the molecular design of PDI derivatives are discussed.

© 2012 Elsevier B.V. All rights reserved.

1. Introduction

A great deal of effort has been devoted to developing efficient solar energy conversion systems [1]. Among them, dye-sensitized solar cells (DSSC) have attracted much attention because of their potential low cost and relatively high power conversion efficiency (η) [2]. Thus far, ruthenium(II) polypyridyl complexes have proven to be the most efficient TiO$_2$ sensitizers, a gradual increment on the highest η value has been recognized in recent years [3,4]. However, in view of cost and environmental demand, metal-free organic dyes are strongly desired for highly efficient dye-sensitized solar cells.

Recently, there are two representative progresses in the development of novel sensitizers for DSSC. One is about ruthenium(II) polypyridyl complexes. Grätzel reported a new heteroleptic polypyridyl ruthenium complexes, with high molar extinction coefficients by extending the π-conjugation of spectator ligands, with a motivation to enhance the optical absorptivity of mesoporous titania film and charge collection yield in a dye-sensitized solar cell [4]. The efficiency of the cells was improved distinctively. The other one is the discovery of organic dyes that contain an electron donor (D) and an acceptor (A) connected via a π-conducting bridge (D–π–A) [5]. The photo-electron conversion efficiencies of the DSSC based on this kind of organic dyes are impressive and

encouraging. A new record of η is achieved by the DSSC based on a D–π–A type of porphyrin has released on literature very recently [6].

Perylenetetracarboxylic diimides (PDI) are well-known for their excellent chemical, thermal, and photophysical stability, and have been utilized in various optical devices [7–9]. Moreover, this kind of dyes usually exhibits a high molar extinction coefficient in visible region ($\sim$10^5 M^{-1} cm^{-1}) [10]. These properties are advantageous for DSSC applications. However, PDIs or similar dyes have rarely been used as sensitizers in DSSC probably because of their strong electron withdrawing ability which is expected to hinder the electron injection to the conduction band of TiO$_2$. Gregg and coworkers have studied the application of a series of perylene mono or diimide dyes as sensitizers for DSSCs [10–12]. Great application potentials are revealed for these kind of compounds despite the lower solar cell efficiency in relative to the traditional polypyridyl ruthenium complex based cell. Edvinsson and Pschirer have presented several novel perylene monoimide dyes with different intramolecular electronic push-pull characters [13]. Based on these dyes, the DSSCs achieved almost 4% solar energy conversion efficiency and a IPCE value up to 70% under AM1.5G irradiation. The performance of this dye is a significant improvement and lifts the performance from modest to promising. Imahori and co-workers have used strong electron-donating group pyrrolidine to decorate the perylene diimide framework, and reduced the electron withdrawing ability of PDI significantly, the solar cell based on this kind of dye presented an energy conversion efficiency of 2.6% [14]. Recently, Li

* Corresponding author. Tel.: +86 0531 8836 9877; fax: +86 0531 8856 4464.
E-mail address: xiyouli@sdu.edu.cn (X. Li).
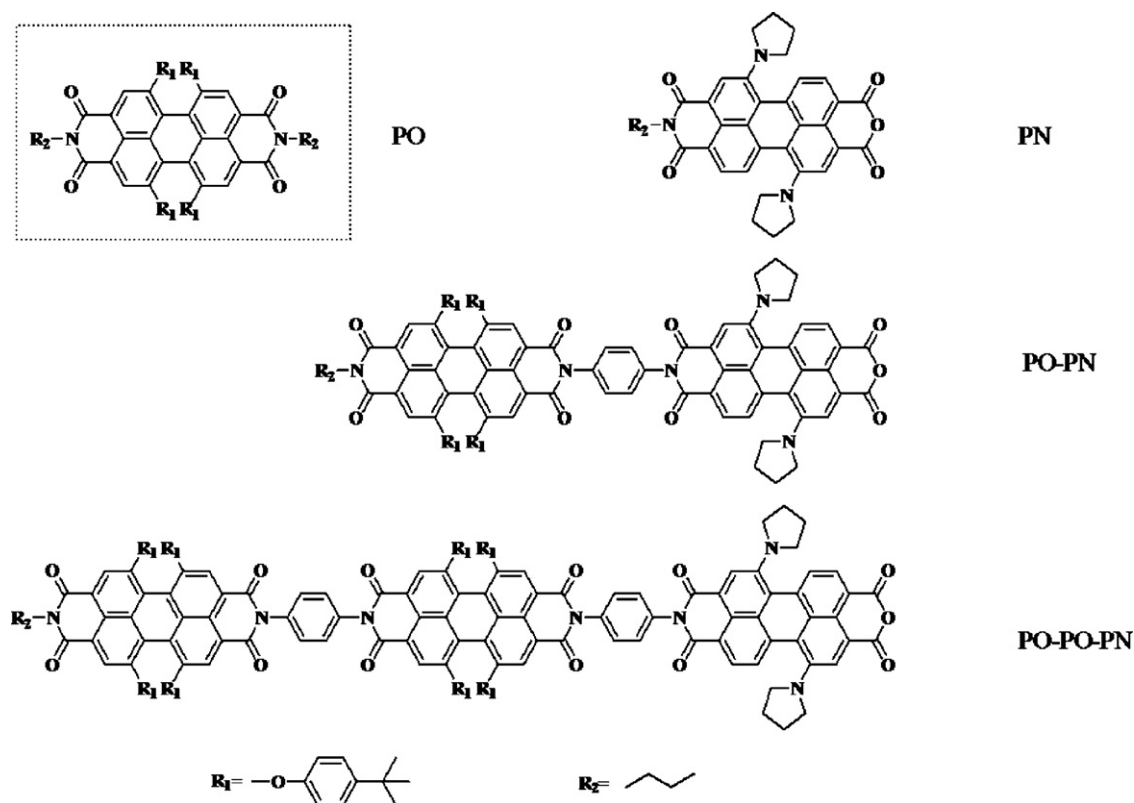
Scheme 1. Structures of the molecules.

and co-workers have successfully designed and synthesized a kind of efficient perylene dye containing two thiophenol groups in the 1 and 6 positions of the perylene framework [15]. The solar energy conversion efficiency of the DSSC based on this kind of dye is as high as 6.8% under AM1.5G solar conditions. More importantly, the solid cell of this kind of dye presents an energy conversion efficiency of 1.8%, suggesting again that perylene dyes are promising sensitizer for DSSCs. All the studies conducted so far on the perylene diimide based DSSC indicate that this kind of compounds are promising sensitizers for DSSC application due to following reasons: (i) the dianhydride group can serve as anchoring group, which can bonding tightly to the surface of titanium dioxide, (ii) the high extinction coefficient ($\approx 4 \times 10^4\,\mathrm{M}^{-1}\,\mathrm{cm}^{-1}$) in the visible region makes it good light harvester, (iii) the excellent stabilities towards heat and light are expected to meet the requirement of a realistic outdoor working solar cell in future, (iv) the molecular structure can be varied easily by introducing substituents at different positions and therefore their sensitizing properties can be promoted further by structure modification.

In this context, we report the synthesis and the photovoltaic characterizations of a series of novel linear PDI-based sensitizers, as shown in Scheme 1. In these compounds, the phenoxy group substituted PDI (PO) units are connected to a pyrrolidinyl group substituted PDI (PN) unit with phenyl bridges. The complementary absorption spectra between POs and PN will in one hand extent the absorption easily to NIR region and on the other hand to increase the overall extinction coefficient throughout the whole absorption spectra. Moreover, the photoinduced energy transfer is expected between PO and PN due to the large overlap between the emission of PO and the absorption of PN and thus the electron injection from the excited state of PN to TiO_2 can be initiated by the photoexcitation of PO.

2. Experimental

2.1. General methods

^{1}H NMR spectra were recorded at 400 MHz with the solvent peak as internal standard (in $CDCl_3$). Electronic absorption spectra were recorded on a Hitachi 4100 spectrometer. Fluorescence spectra were measured on an ISS K2 system. Fluorescence quantum yields were calculated with N,N′-dicyclohexylperylene-3,4:9,10-tetracarboxylic diimide ($\Phi_f = 100\%$) as standard. MALDI-TOF mass spectra were obtained on Bruker BIFLEX III mass spectrometer with α-cyano-4-hydroxycinnamic acid as matrix. The thermogravimetric analysis was conducted on a SDT Q600 instrument. The IPCE values were determined by Zolix Solar Cell Scan 100 (Solar Cell QE/IPCE Measurement System) and the photocurrent–voltage characteristics were done under 100 mW cm^{-2} light intensity and AM1.5 conditions. A Xenon light source was used to produce an irradiance of various intensities. I–V data collection was made by using CHI-660D CH Instruments Electrochemical Workstation. All the experimental data were given as an average from three independent measurements.

2.2. Materials

[N,N′-dicyclohexyl-1,7-di(pyrrolidinyl)]perylene-3,4:9,10-tetracarboxylic diimide **(1)**, [16] and [N,N′-dicyclohexyl-1,6,7,12-tetra(p-t-butyl)phenoxyl]perylene-3,4:9,10-tetracarboxylic diimide **(2)** were prepared following the literature methods [17]. 1,6,7,12-Tetra(4-t-butylphenoxy)perylene-3,4:9,10-tetracarboxylic dianhydride and 1,7-di(pyrrolidinyl)]perylene-3,4:9,10-tetracarboxylic dianhydride were prepared by the hydrolysis of corresponding diimides in n-propanol and

potassium hydroxide according to the published procedures [18]. N-n-butyl-1,6,7,12-tetra(4-t-butylphenoxy) perylene-3,4:9,10-tetracarboxylic-3,4-anhydride-9,10-imide **(3)** [19] and N-n-butyl-1,7-di(pyrrolidinyl)]perylene-3,4:9,10-tetracarboxylic-3,4-anhydride-9,10-imide **(4)** [20] were prepared following the literature method. The compounds above were fully characterized by ^{1}H NMR and MALDI-TOF mass spectra.

All other chemicals are purchased from commercial source. Solvents were of analytical grades and were purified by the standard method before use.

2.3. Synthesis

2.3.1. N-n-butyl-N-p-phenylenediamine-1,6,7,12-tetra(4-tert-butylphenoxy)perylene-3,4:9,10-tetracarboxylic diimide (5)

N-n-butyl-1,6,7,12-tetra(4-tert-butylphenoxy)perylene-3,4:9,10-tetracarboxylic-3,4-anhydride-9,10-imide (156 mg, 0.15 mmol), p-phenylenediamine (20 mg, 0.18 mmol) in 50 ml of pyridine were refluxed for 36 h. After the solvent was evaporated, the residue was chromatographed on silica gel using $CHCl_3/MeOH$ (1000:1,v/v) as the eluent. After recrystallization from chloroform and methanol, the product was collected as purple solid (130 mg, 79%). Mp. > 300 °C; ^{1}H NMR (300 MHz, CDCl$_3$, 25 °C, TMS): 8.27 (s, 2H), 8.21 (s, 2H), 7.36 (s, 4H), 7.24 (m, 8H), 6.82 (m, 8H), 4.11 (t, 2H), 1.65 (m, 2H), 1.37 (m, 2H), 1.29 (s, 36H), 0.93 (t, 3H). MS (MALDI-TOF): m/z, calculated for $C_{74}H_{71}N_3O_8$: 1130.37, found 1130.31 [M$^+$].

2.3.2. Compound 6

A mixture of N-n-butyl-N-p-phenylenediamine-1,6,7,12-tetra(4-tert-butylphenoxy) perylene-3,4:9,10-tetracarboxylic diimide **(5)** (150 mg, 0.13 mmol), imidazole (1.5 g), and 1,6,7,12-tetra(4-t-butylphenoxy)perylene-3,4:9,10-tetracarboxylic acid anhydride (260 mg, 0.26 mmol) in toluene (15 ml) was heated to reflux and kept at reflux for 48 h. The solvents were removed under reduced pressure and the residue was washed with water. The product was purified by column chromatography on silica gel with chloroform/petroleum ether (10:1, v/v) as eluent. After recrystallization from chloroform and methanol, the product was collected as red solid (45 mg, 30%). Mp. > 300 °C; ^{1}H NMR (300 MHz, CDCl$_3$, 25 °C, TMS): 8.22 (m, 8H), 7.36 (s, 4H), 7.23 (m, 16H), 6.83 (m, 16H), 4.11 (t, 2H), 1.64 (m, 2H), 1.40 (m, 2H), 1.28 (m, 72H), 0.93 (t, 3H). MS (MALDI-TOF): m/z, calculated for $C_{138}H_{125}N_3O_{17}$: 2097.48, found 2098.01 [M$^+$].

2.3.3. N-p-phenylenediamine-1,7-di(pyrrolidinyl)]perylene-3,4:9,10-tetracarboxylic-3,4-anhydride-9,10-imide (7)

A mixture of 1,7-di(pyrrolidinyl)perylene-3,4:9,10-tetracarboxylic acid anhydride (106 mg, 0.2 mmol) and p-phenylenediamine (21 mg, 0.2 mmol) in 50 ml of pyridine were refluxed for 12 h. After the solvent was evaporated, the residue was chromatographed on silica gel using $CHCl_3/MeOH$ (1000:5, v/v) as the eluent. After recrystallization from chloroform and methanol, the product was collected as green solid (18 mg, 15%). Mp. > 300 °C; ^{1}H NMR (300 MHz, CDCl$_3$, 25 °C, TMS): 8.52 (s, 1H), 8.42 (s, 1H),8.44 (d, 1H), 8.39 (d, 1H), 7.69 (d, 1H), 7.55 (d, 1H), 7.09, 7.11 (d, 2H), 6.84 (d, 2H), 2.05 (d, 8H), 2.83 (s, 4H), 3.74 (s, 4H). MS (MALDI-TOF): m/z, calculated for $C_{38}H_{28}N_4O_5$: 620.65, found 620.484 [M$^+$].

2.3.4. Compound PO–PN

A mixture of N-n-butyl-1,6,7,12-tetra(4-tert-butylphenoxy) perylene-3,4:9,10-tetra carboxylic-3,4-anhydride-9,10-imide (100 mg, 0.1 mmol), imidazole (600 mg), and N- p-phenylenediamine-1,7-di(pyrrolidinyl)]perylene-3,4:9,10-tetracarboxylic-3,4- anhydride-9,10-imide (62 mg, 0.1 mmol) in toluene (50 ml) was heated to reflux and kept at reflux for 24 h. The solvents were removed under reduced pressure and the residue was washed with water. The product was purified by column chromatography on silica gel with chloroform/methanol (1000:1, v:v) as eluent. The second dark purple fraction contained PO–PN. After recrystallization from chloroform and methanol, the product was collected as black solid (15 mg, 9.1%). Mp. > 300 °C; ^{1}H NMR (300 MHz, CDCl$_3$, 25 °C, TMS): 8.48 (m, 4H), 8.28 (s + s, 4H), 7.78 (d, 1H), 7.64 (d, 1H), 7.45 (m, 4H), 7.23 (m, 8H), 6.86 (m, 8H), 4.12 (t, 2H), 3.76 (br, 4H), 2.86 (br, 4H), 2.11 (br, 8H), 1.69 (m, 2H), 1.39 (m, 2H), 1.29 (m, 36H), 0.94 (t, 3H). MS (MALDI-TOF): m/z, calculated for $C_{106}H_{91}N_5O_{13}$: 1642.88, found 1642.66 [M$^+$]. Elemental analysis (%) calculated for $C_{106}H_{91}N_5O_{13}$: C 77.49, H 5.58, N 4.26; found: C 76.57, H 5.62, N 4.18.

2.3.5. Compound PO–PO–PN

By employing the similar procedures of compound PO–PN using compound **6** (60 mg, 0.03 mmol) instead of N-n-butyl-1,6,7,12-tetra(4-tert-butylphenoxy)perylene- 3,4:9,10-tetracarboxylic-3,4-anhydride-9,10-imide as starting material, compound PO–PO–PN was prepared. The product was purified by column chromatography on silica gel with chloroform/methanol (1000:1.5, v/v) as eluent. The first dark purple fraction contained PO–PO–PN. After recrystallization from chloroform and methanol, the product was collected as black solid (7.3 mg, 9.5%). Mp. > 300 °C; ^{1}H NMR (300 MHz, CDCl$_3$, 25 °C, TMS): 8.43(m, 4H), 8.24(m, 8H), 7.61–7.74(d + d, 2H), 7.45(s, 4H), 7.38(s, 4H), 7.22(m, 16H), 6.85(m, 16H), 4.11(t, 2H), 3.76(br, 4H), 2.86(br, 4H), 2.12(br,8H), 1.64(m, 2H), 1.40(m, 2H), 1.29(m, 72H), 0.93(t, 3H). MS(MALDI-TOF): m/z, calculated for $C_{176}H_{151}N_7O_{21}$: 2700.12, found 2702.423 [M$^+$]. Elemental analysis (%) calculated for $C_{176}H_{151}N_7O_{21}$: C 76.72, H 5.64, N 3.63; found: C 74.40, H 5.53, N 3.42.

2.4. Fabrication of solar cells

The TiO$_2$ electrodes (purchased from Dalian Heptachroma Co., Ltd) consist of an adsorbent mesoporous layer of anatase TiO$_2$ particles (average size 20 nm) with a thickness of 12 μm and a second light scattering layer anatase TiO$_2$ (average particle size 200 nm) with a thickness of 2 μm. The surface area of the TiO$_2$ electrode was 0.36 cm^2. Platinized FTO glasses were used as a counter electrode. The TiO$_2$ electrodes were immersed into the solutions of the three dyes (0.3 mM) above in CH$_2$Cl$_2$ and kept at room temperature for 15 h. After dye adsorption, the dye-coated electrodes were copiously rinsed with the same solvent used for the adsorption. The TiO$_2$ electrodes loaded with dye exhibit green color for the PN dyes and a black color for the PO–PN and PO–PO–PN dyes. The dye-adsorbed TiO$_2$ electrode and platinized counter electrode were assembled into a sealed sandwich-type cell with a gap of a hot-melt ionomer film (Surlyn 1702, thickness 25 μm, DuPont). The electrolyte solution consists a mixture of 0.6 M 2,3-dimethyl-1-propyl imidazolium iodide, 0.05 M I$_2$, 0.1 M LiI in acetonitrile. For comparison purpose, several experiments were also performed with 0.5 M 4-t-butylpyridine in the electrolyte (see Table 3).

3. Results and discussion

3.1. Synthesis

The synthetic scheme is shown in Scheme 2. In brief, the PDI molecules were linked through p-phenylenediamine at their imide positions via condensation of the resulting aminoimide **(7)** with the appropriate mono- or dianhydride. All the new compounds were fully characterized with ^{1}H NMR, MALDI-TOF mass spectra, as well
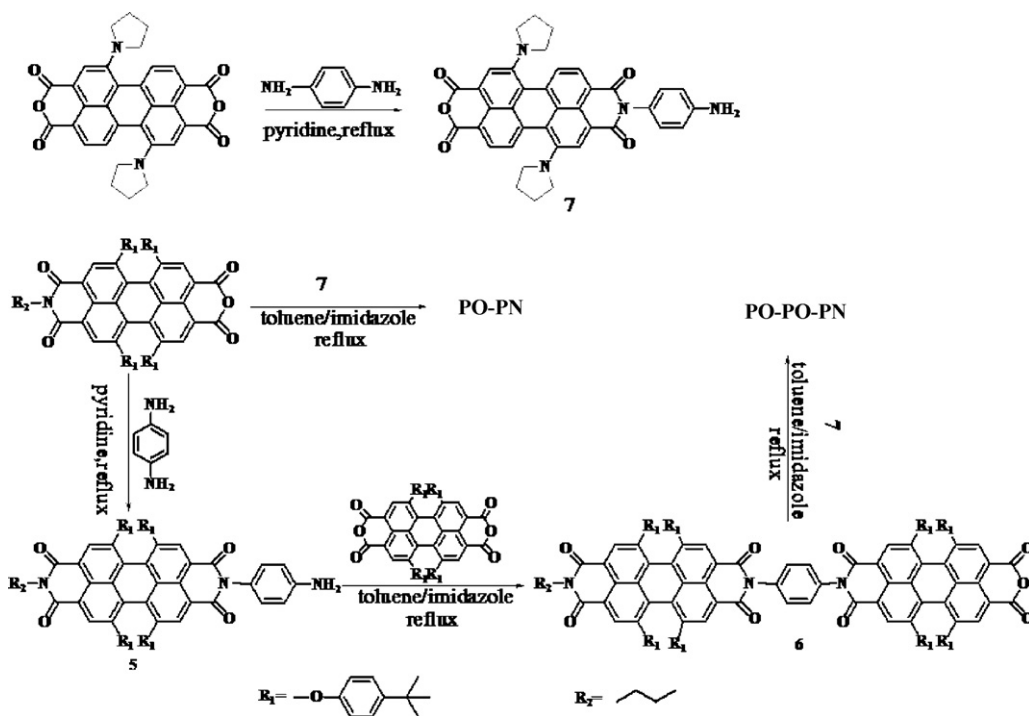
Scheme 2. Synthesis of the molecules.

as elemental analysis. All the compounds show excellent stabilities towards heat as revealed by the thermogravimetric analysis (supporting information, Fig. S6).

3.2. UV–Vis absorption spectroscopy

The electronic absorption spectra of PN, PO–PN, PO–PO–PN and the reference compound PO in CH_2Cl_2 are presented in Fig. 1(A) and (B), respectively. Fig. 1(A) compares the absorption spectra of PO–PN with that of monomer PO and PN. The spectrum of PO–PN is almost identical to that of the 1:1 mixture of PO and PN. This result indicates that no strong electronic interactions between the PO and PN units at the ground states. However, the absorption spectra of PO–PO–PN shown in Fig. 1(B) states that the maximal absorption band at about 585 nm, which is attributed to the absorption of PO units is red-shifted for about 5 nm in relative to that of the reference compound PO. This result suggests that there are weak "J-type" interactions between the PO units in PO–PO–PN at ground states [21].

Table 1 summarizes the UV/vis absorption properties of these compounds in CH_2Cl_2 and toluene. The absorption spectra of these compounds in toluene and in CH_2Cl_2 are almost identical except a slight bathochromic shift of a few nanometers when going from toluene to CH_2Cl_2. This can be attributed to the stabilizing effect of the larger polarity of CH_2Cl_2 to the excited states. It is noteworthy that these multichromophore compounds (the black line with closed circles in Fig. 1) absorb strongly across a very large wavelength range of visible light with high extinction co-efficient ($\varepsilon > 10^4\,M^{-1}\,cm^{-1}$), which are believed to be advantageous for DSSC applications.

The normalized absorption spectra of PN, PO–PN, PO–PO–PN in CH_2Cl_2 and absorbed on TiO_2 electrodes are compared in Fig. 2. Fig. 2(A) shows the UV/Vis absorption spectra of PN in CH_2Cl_2 solution or adsorbed on a TiO_2 electrode. The notable increase in the absorption of PN at around 650 nm reveals the occurrence of the dye aggregation on the TiO_2 electrode [22]. More importantly, a blue shift on the most right edge of the absorption spectra of PN on

TiO_2 in relative to that in solution is observed, this maybe attributed to the ring opening of the anhydride group on the perylene to form two carboxylates, which provide strong chemical interactions with the oxide surface. This phenomenon is well known for other perylene anhydride sensitizers [13,23]. The absorption spectra of PO–PN and PO–PO–PN reveal similar aggregation behavior for
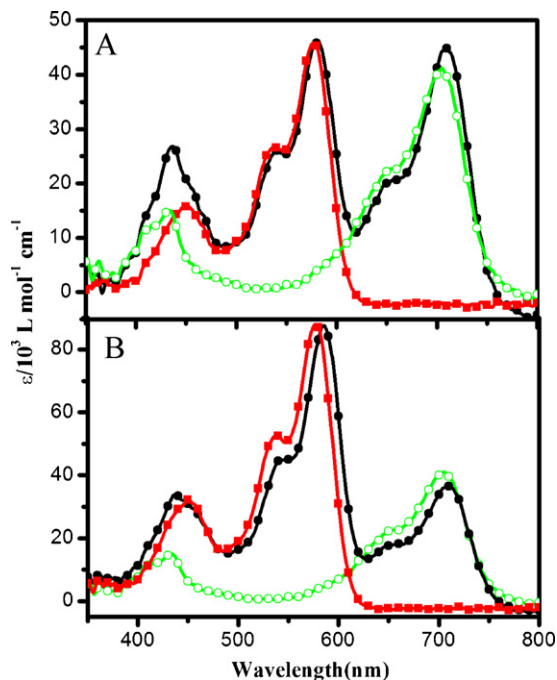

Fig. 1. UV–vis absorption spectra of PN (green line with open circles), PO–PN (black line with closed circles in A), PO–PO–PN (black line with closed circles in B) and the reference compound PO (red line with closed squares) in CH_2Cl_2. (Note: the absorption spectrum of PO in B is normalized with that of PO–PO–PN for comparison purpose.). (For interpretation of the references to color in this figure legend, the reader is referred to the web version of this article.)

Table 1
The UV/Vis absorption properties of the compounds.

Compound	λ, nm ($\varepsilon/10^4$ L mol^{-1} cm^{-1})	
	CH$_2$Cl$_2$	Toluene
PO	449(1.55) 537(2.67) 578(4.55)	446(1.96) 534(3.11) 572(5.04)
PN	433(1.44) 702(4.06)	429(1.56) 688(3.80)
PO–PN	435(2.70) 539(2.59) 580(4.55) 707(4.43)	432(2.98) 534(3.01) 575(4.99) 702(4.38)
PO–PO–PN	437(3.39) 542(4.44) 584(8.77) 708(3.63)	432(4.02) 536(5.24) 578(9.69) 702(4.07)

them on the surface of TiO$_2$. However, the absorption of PO–PN and PO–PO–PN on the surface of TiO$_2$ in the region of 420–620 nm has been enhanced signifncalty compared with that of PN. In an other words, PO–PN and PO–PO–PN show impressively wide absorption window in the whole visible wavelength range and enhance the optical absorption of mesoporous titania film and light collecting efficiency significantly.

3.3. Photoinduced energy transfer from PO to PN

Fig. 3 shows the fluorescence spectra of PO–PN in CH$_2$Cl$_2$ with excitation at 510 nm. At this wavelength, the absorption of PO is five times larger than that of PN, therefore the excitation at this wavelength is thoroughly considered to be a selective excitation to the PO units in compounds PO–PN and PO–PO–PN.

As expected, the fluorescence of the PO part in PO–PN, appears around 610 nm, is extremely small. This indicates that the fluorescence of PO in PO–PN is quenched significantly. The strong emission band centered at about 747 nm can be attributed to the fluorescence of PN unit, which suggests strongly that the photoinduced energy transfer happened from PO to PN within PO–PN. This has further proved by the excitation spectra of PO–PN while the emission at 747 nm is monitored (Fig. 4). The excitation spectrum of
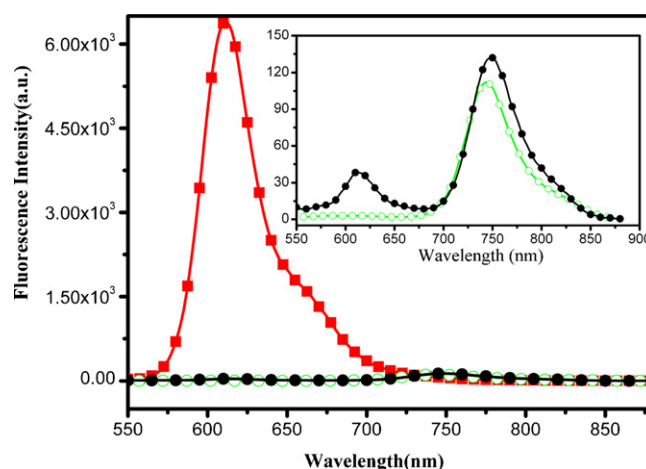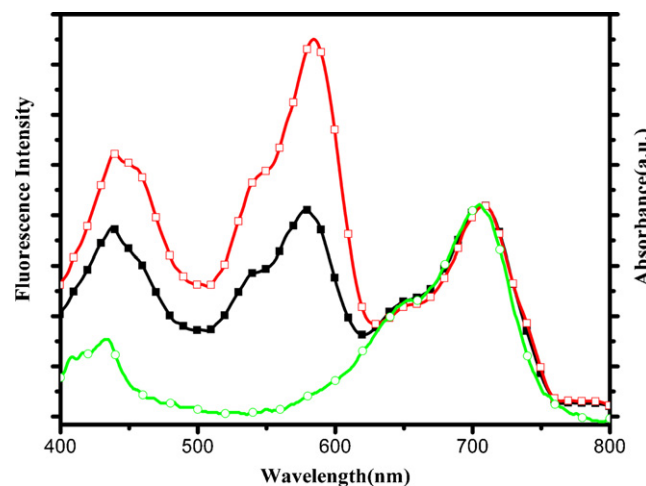

Fig. 3. Fluorescence spectra of PO–PN (black line with closed circles), PO (red line with closed squares), PN (green line with open circles) in CH$_2$Cl$_2$ (5×10^{-6} mol L^{-1}, $\lambda_{ex} = 510$ nm). The inset compares the fluorescence spectra of PO–PN and PN at the same concentration. (For interpretation of the references to color in this figure legend, the reader is referred to the web version of this article.)

PO–PN shows a pronounced PO absorption feature in the region of 500–625 nm. This observation suggests that the absorption of PO contribute to the fluorescence of PN to a remarkable extent and indicates the presence of the singlet–singlet energy transfer from PO to PN within PO–PN. Similar results can be deduced from the fluorescence spectra (Fig. S2 in supporting information) and excitation spectra (Fig. 4) of PO–PO–PN.

The energy transfer from PO to PN within both PO–PN and PO–PO–PN can be rationalized by the good overlap between the fluorescence of PO and the absorption of PN as shown in Fig. 5. The
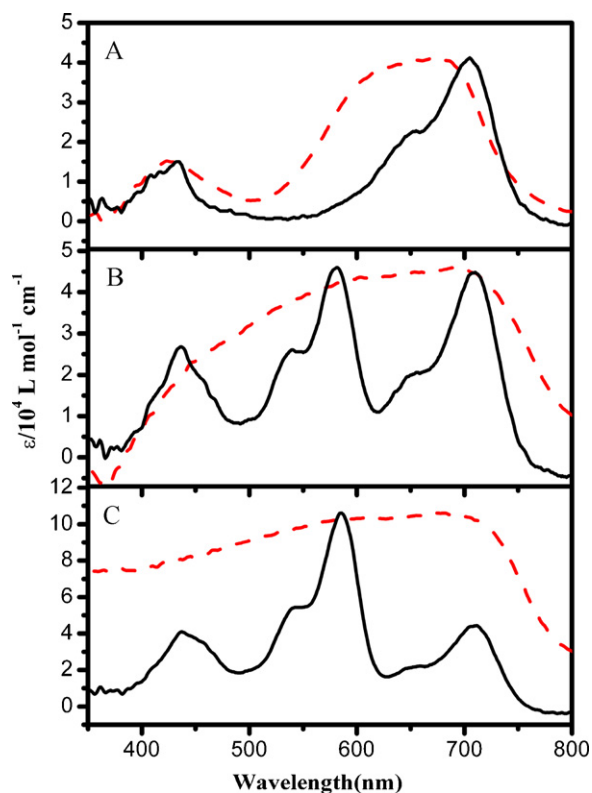
Fig. 2. Normalized absorption spectra of PN (A), PO–PN (B), PO–PO–PN (C) in CH$_2$Cl$_2$ (solid line) and absorbed on the TiO$_2$ electrodes (dashed line). The absorption arising from the TiO$_2$ electrode was subtracted from the spectrum.

Fig. 4. The normalized excitation spectra of PO–PN (black line with closed squares), PO–PO–PN (red line with open squares) monitoring at 747 nm compared with the absorption spectra of PN (green line with open circles) in CH$_2$Cl$_2$. (For interpretation of the references to color in this figure legend, the reader is referred to the web version of this article.)
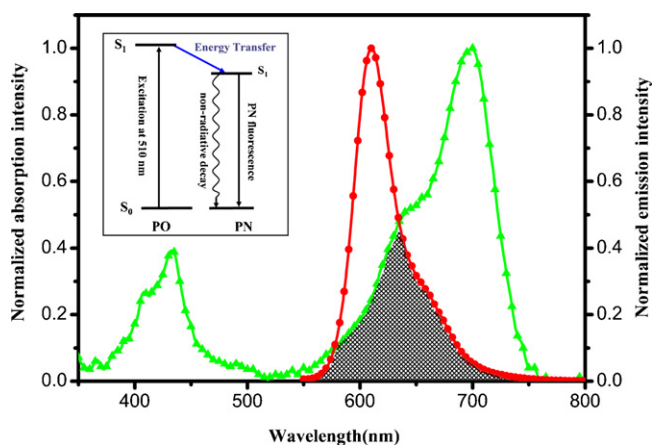
Fig. 5. The overlap (shadow area) between the absorption of PN (green line with closed triangles) and the fluorescence of PO (red line with closed circles). The inset shows the relative energy levels of the excited states of PO and PN. (For interpretation of the references to color in this figure legend, the reader is referred to the web version of this article.)

diagram of the relative energy levels of the excited states of PO and PN as shown in the inset of Fig. 5 suggests further that the above mentioned energy transfer is theoretically possible process. The selective excitation at PO unit of PO–PN and PO–PO–PN leads to the formation of PO-based π-π^* excited states, which is followed by an energy transfer to the lowest-lying PN-based singlet excited states. So the fluorescence of the PO is greatly diminished by the presence of the covalently attached PN. The PN-based singlet excited states undergo deactivation either to the ground state by radiative decay (fluorescence) or by non-radiative decay. It is worth noting that, the fluorescence intensity of PO–PN and PO–PO–PN at 747 nm as shown in Figs. 3 and S2 is very small, which is caused by the intrinsic small fluorescence quantum yield of PN. The introduction of electron-donating pyrrolidinyl groups at the 1,7 positions of PDI core leads to charge transfer characteristics for the excited states of PN molecules, which in turn results in a significant decrease on the fluorescence quantum yield [24].

The energy transfer efficiency (Φ_{ent}) calculated from the fluorescence quenching efficiency (Φ_q) is about 100%. Similar results can also be deduced from the fluorescence spectra of PO–PO–PN (Supporting Information). The data of fluorescence spectra of PO–PN and PO–PO–PN are summarized in Table 2. The energy transfer from PO unit to PN in both PO–PN and PO–PO–PN is efficient and this good light harvesting effect is expected to be advantageous for solar energy conversion efficiency.

3.4. Photovoltaic device performance

The photovoltaic performances of these dyes were investigated with two electrolytes that differ only by the presence or the absence of 4-tert-butylpyridine (Table 3). The current–voltage characteristics were measured under AM 1.5 conditions (100 mW cm^{-2}). Figs. 6 and S5 (supporting information) show the current–voltage characteristics with electrolyte A and B, respectively. The η values

Table 2
Fluorescence properties of the compounds (excited at 510 nm).

	Solvent	PO	PO–PN PO	PO–PO–PN PO
Φ_f (510) (%)	CH$_2$Cl$_2$	80.2	1.91	1.12
	Toluene	81.1	0.25	0.17
Φ_q (%)	CH$_2$Cl$_2$	–	98	98
	Toluene	–	99	99

Table 3
Cell performance of these dyes-sensitized TiO$_2$ cells.

Dye	Electrolyte[a]	V_{OC} (V)	J_{SC} (mA cm^{-2})	ff	η (%)
PN	A	0.55	1.37	0.62	0.44
	B	0.35	1.90	0.52	0.35
PO–PN	A	0.55	1.21	0.64	0.40
	B	0.34	1.64	0.54	0.30
PO–PO–PN	A	0.53	1.10	0.63	0.35
	B	0.35	1.38	0.55	0.26

[a] Electrolyte A: 0.6 M 2,3-dimethyl-1-propyl imidazolium iodide, 0.05 M I$_2$, 0.1 M LiI and 0.5 M 4-t-butylpyridine in acetonitrile. Electrolyte B: 0.6 M 2,3-dimethyl-1-propyl imidazolium iodide, 0.05 M I$_2$, 0.1 M LiI in acetonitrile.

are derived from the equation $\eta = V_{OC} \times J_{SC} \times ff$, where V_{OC} is open circuit potential (V), J_{SC} is short circuit current density (mA cm^{-2}), and ff is the fill factor (Table 3). The overall photovoltaic conversion efficiencies are different and can be ranked in the order of PN > PO–PN > PO–PO–PN in two kinds of different electrolyte solution. It is clear that the preparation of the photovoltaic devices is not optimized since the PN sensitizer gives much lower overall photoconversion efficiency than that reported in literature [14]. However, the present results permit to compare the dyes between each other and to draw information regarding the factors that affect their relative performance. Moreover, it's obvious that addition of 4-tert-butylpyridine to the electrolyte gives an improvement of the solar cells as is well-documented in the literature [25–29]. The main effects of 4-tert-butylpyridine are improving the open-circuit potential (V_{OC}) and decreasing the short-circuit current slightly. The increases of the V_{OC} could be attributed to a shift of the TiO$_2$ band edge toward negative potentials [30].

Fig. 7 shows the incident monochromatic photon-to-current conversion efficiency (IPCE) curve for the solar cell sensitized with PN, PO–PN, and PO–PO–PN. As seen from the IPCE spectra of PN, PO–PN and PO–PO–PN, the change of the IPCEs is a complete linearity with comparison to overall conversion efficiencies and short circuit currents as shown in Table 3. The photocurrent action spectra of the solar cells of PO–PN and PO–PO–PN exhibit broader band in the red-to-NIR region in comparison with that of the device of PN. This unambiguously supports that the PO units within PO–PN and PO–PO–PN contribute to the photocurrent generation. The contribution of PO in PO–PO–PN and PO–PN to the photocurrent is more distinctively revealed by the normalized photocurrent action spectra in the range of 420–640 nm (supporting information Fig. S4). Moreover, the relative contribution of PO for the photocurrent in PO–PO–PN is larger than that in PO–PN, which obviously due to the more donor PO units in PO–PO–PN. The overall mechanism for
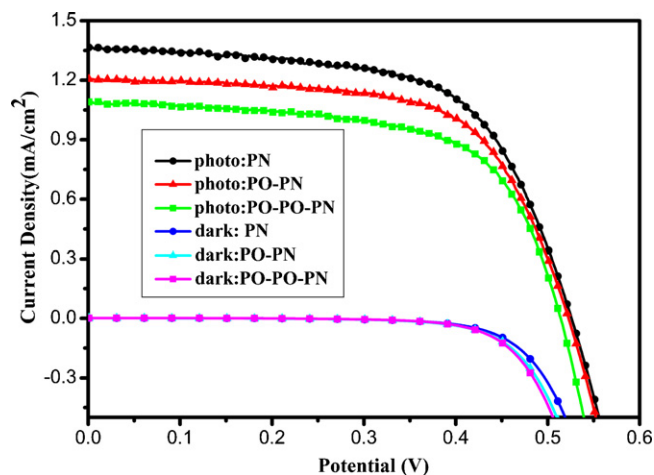
Fig. 6. Current–Voltage characteristics of PN, PO–PN, PO–PO–PN with electrolyte A under simulated solar illumination (AM 1.5G) and in dark.
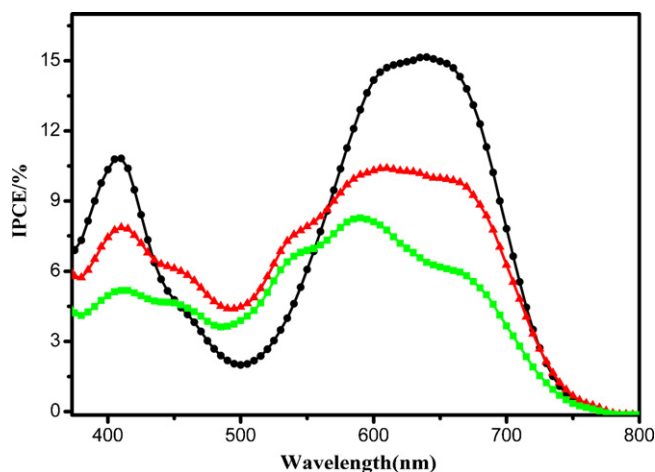
Fig. 7. Action spectra of PN (black line with closed circles), PO–PN (red line with closed triangles) and PO–PO–PN (green line with closed squares) sensitized TiO$_2$ cells. (For interpretation of the references to color in this figure legend, the reader is referred to the web version of this article.)

Table 4
Fluorescence properties of the compounds (PN is selectively excited at 630 nm).

| Compound	Solvent	PN	PO–PN PN	PO–PO–PN PN
Φ_f (630) (%)	CH$_2$Cl$_2$	2.16	1.82	1.55
	Toluene	3.6	3.2	3.08
Φ_{ET} (%)	CH$_2$Cl$_2$	–	15.7	28.2
	Toluene	–	11.1	14.4

Table 5
Calculated free-energy changes ΔG_{ET}^0 of the photoinduced electron transfer within PO–PN, PO–PO–PN.

Compound		PO$_1$–PN	PO$_2$–PO$_1$–PN
r_{DA} (Å)		PO$_1$–PN 16.93	PO$_2$–PN 34.80
ΔG_{ET}^0 (ev)	Toluene	−0.25	−0.07
	CH$_2$Cl$_2$	−0.38	−0.34

the generation of photocurrent can be schematically illustrated as Fig. 8. Photo excitation at PO leads to the singlet excited states of PO, which then conducts a singlet energy transfer to PN and produces a singlet excited states of PN. Electron injections take place from PN singlet excited states to the conduction band of titanium dioxide and finally generate photocurrent in out circle. This result demonstrated for the first time that the intramolecular singlet–singlet energy transfer is a reliable strategy to improve the light harvesting abilities of a dye adsorbed on titania films. The relatively high IPCE values at 600–800 nm are particularly intriguing because of their possible applications in transparent solar cells for windows and tandem cells [14].

However, the overall solar energy conversion efficiencies are inconsistent with what we anticipated above. The unexpected drop on overall solar energy conversion efficiencies after the introduction of PO reminds us that an extra unfavorable process, which hinder the electron injection from the excited state of PN to the conduction band (CB) of the TiO$_2$ electrode. To confirm this

prognosis, the fluorescence quantum yields of these three compounds in different solvents are calculated when PN unit was selectively excited at 630 nm. The results are summarized in Table 4. The fluorescence quantum yields of PN within PO–PN and PO–PO–PN are distinctively smaller than that of compound PN, indicating that PO quenches the fluorescence of PN too. The most likely process by which the fluorescence of PN is quenched in these compounds is electron transfer from PN to PO.

The free energy changes (ΔG_{ET}^0) of the electron transfer from PN to PO in these compounds are estimated following the reference [31]. The calculated free energy changes for the compounds are all negative and the electron transfer from PN to PO are thermal dynamically favorable reactions (Table 5). This electron transfer process corresponds very well to the low fluorescence intensity recorded experimentally for PN as shown in Fig. 3.

The electron transfer efficiencies (Φ_{ET}) are calculated according to the reference method [31] and the results are summarized in Table 4. It is clear that the electron transfer efficiency gradually increases in PO–PN, PO–PO–PN. This corresponds well with the decreasing of the solar energy conversion efficiencies following the order of PN > PO–PN > PO–PO–PN.
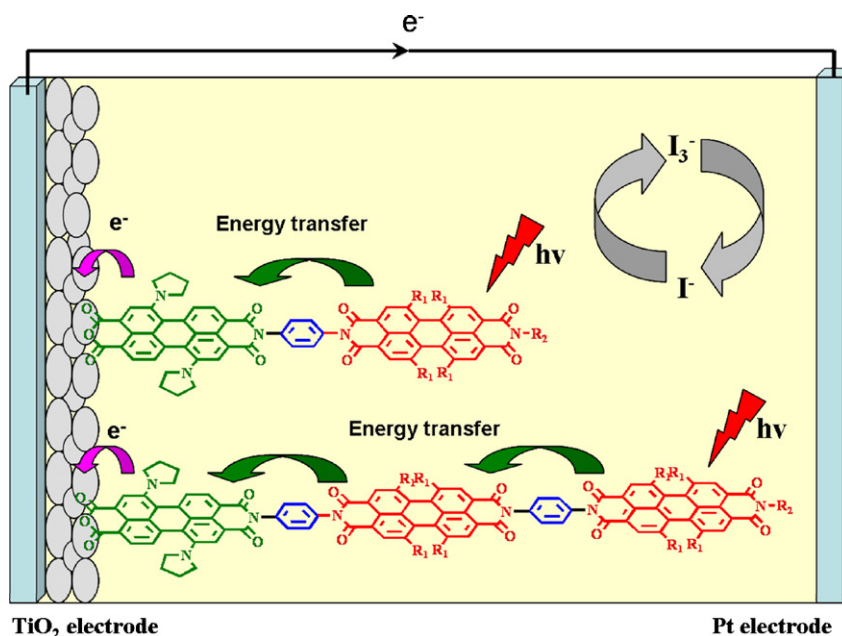
Fig. 8. Schematic representation of the mechanism of the photocurrent generation.

Therefore, two controversial factors affect the solar energy conversion efficiencies of solar cell within PO–PN and PO–PO–PN. The energy transfer from PO to PN favors the solar energy conversion process while the electron transfer from PN to PO is unfavorable to the solar energy conversion. Obviously the effect of unfavorable electron transfer in PO–PN and PO–PO–PN overwhelms that of favorable energy transfer and consequently the overall solar energy conversion efficiency is reduced. The cell performance would be improved significantly if the electron transfer from PN to PO were avoided.

4. Conclusions

In conclusion, we have successfully synthesized a series of novel rigid and linear PDI-based donor-acceptor derivatives with varied number of PO units and an anhydride as the strong coupling group for dye-sensitized solar cells. These PDIs have broad absorptions in the visible-to-NIR region, showing that they are excellent light harvesting molecules. In these compounds, when the PO units were selectively excited, photoinduced intramolecular energy transfer proceeded efficiently from the excited PO units to the PN unit. The IPCE spectra unequivocally corroborate that the introduction of the donor PO is responsible for the significant improvement of the cell performance in the range of 420–640 nm in relative to that in the region around 700 nm, although the overall solar energy conversion efficiency decreased in the order of PN, PO–PN, PO–PO–PN owing to the unexpected electron transfer. It is obvious that the cell performance would be improved, if the electron transfer from PN to PO were avoided by modifying the dye molecules and optimize the preparation of the photovoltaic devices. We believe that this information is useful for the development of new generation of PDI sensitizers for DSSC.

Acknowledgements

Appendix A. Supplementary data

Supplementary data associated with this article can be found, in the online version, at http://dx.doi.org/10.1016/j.jphotochem.2012.04.019.

References

[1] (a) V. Balzani, M. Venturi, A. Credi, Molecular Devices and Machines – A Journey into the Nano World, Wiley-VCH, Weinheim, 2003;
(b) S.-S. Sun, N.S. Sariciftci, Organic Photovoltaics, CRC Press, Boca Raton, 2005.
[2] (a) B. O'Regan, M. Grätzel, A low-cost, high-efficiency solar cell based on dye-sensitized colloidal TiO_2 films, Nature 353 (1991) 737–740;
(b) B.A. Gregg, Excitonic solar cells, Journal of Physical Chemistry B 107 (2003) 4688–4698;
(c) M.K. Nazeeruddin, Special issue on dye-sensitized solar cells, Coordination Chemistry Reviews 248 (2004) 1161–1164;
(d) M. Grätzel, Solar energy conversion by dye-sensitized photovoltaic cells, Inorganic Chemistry 44 (2005) 6841–6851;
(e) J.R. Durrant, S.A. Haque, E. Palomares, Photochemical energy conversion: from molecular dyads to solar cells, Chemical Communications 31 (2006) 3279–3289.
[3] M.K. Nazeeruddin, F. De-Angelis, S. Fantacci, A. Selloni, G. Viscardi, M. Grätzel, Combined experimental and DFT-TDDFT computational study of photoelectrochemical cell ruthenium sensitizers, Journal of the American Chemical Society 127 (2005) 16835–16847.
[4] F. Gao, Y. Wang, D. Shi, J. Zhang, M. Wang, S.M. Zakeeruddin, M. Grätzel, Enhance the optical absorptivity of nanocrystalline TiO_2 film with high molar extinction coefficient ruthenium sensitizers for high performance dye-sensitized solar cells, Journal of the American Chemical Society 130 (2008) 10720–10728.
[5] M. Grätzel, Recent advances in sensitized mesoscopic solar cells, Accounts of Chemical Research 42 (2009) 1788–1798.
[6] A. Yella, M. Grätzel, Porphyrin-sensitized solar cells with Cobalt(II/III)-based redox electrolyte exceed 12 percent efficiency, Science 334 (2011) 629–634.
[7] (a) C. Ego, D. Marsitzky, S. Becker, J. Zhang, A.C. Grimsdale, H. Müllen, R.H. Friend, Attaching perylene dyes to polyfluorene: three simple, efficient methods for facile color tuning of light-emitting polymers, Journal of the American Chemical Society 125 (2003) 437–443;
(b) S. Alibert-Fouet, S. Dardel, H. Bock, M. Oukachmih, S. Archambeau, I. Seguy, P. Destruel, Electroluminescent diodes from complementary discotic benzoperylenes, ChemPhysChem 4 (2003) 983–985.
[8] (a) Y. Liu, Y. Li, L. Jiang, H. Gan, H. Liu, D. Zhu, Assembly and characterization of novel hydrogen-bond-induced nanoscale rods, Journal of Organic Chemistry 69 (2004) 9049–9054;
(b) W.S. Shin, H.-H. Jeong, M.-K. Kim, S.-H. Jin, M.-R. Kim, J.-K. Lee, Y.-S. Gal, Effects of functional groups at perylene diimide derivatives on organic photovoltaic device application, Journal of Materials Chemistry 16 (2006) 384–390.
[9] (a) M.P. O'Neil, M.P. Niemczyk, W.A. Svec, D. Gosztola, G.L. Gaines, M.R. Wasielewski, Picosecond optical switching based on biphotonic excitation of an electron donor-acceptor-donor molecule, Science 257 (1992) 63–65;
(b) L. Zang, R. Liu, M.W. Holman, K.T. Nguyen, D.M. Adams, A single-molecule probe based on intramolecular electron transfer, Journal of the American Chemical Society 124 (2002) 10640–10641.
[10] S. Ferrere, A. Zaban, B.A. Gregg, Dye sensitization of nanocrystalline tin oxide by perylene derivatives, Journal of Physical Chemistry B 101 (1997) 4490–4493.
[11] S. Ferrere, B.A. Gregg, Large increases in photocurrents and solar conversion efficiencies by UV illumination of dye sensitized solar cells, Journal of Physical Chemistry B 105 (2001) 7602–7605.
[12] S. Ferrere, B.A. Gregg, New perylenes for dye sensitization of TiO_2, New Journal of Chemistry 26 (2002) 1155–1160.
[13] T. Edvinsson, C. Li, N. Pschirer, J. Schoneboom, F. Eickemeyer, A. Hagfeldt, Intramolecular charge-transfer tuning of perylenes: spectroscopic features and performance in dye-sensitized solar cells, Journal of Physical Chemistry C 111 (2007) 15137–15140.
[14] Y. Shibano, T. Umeyama, Y. Matano, H. Imahori, Electron-donating perylene tetracarboxylic acids for dye-sensitized solar cells, Organic Letters 9 (2007) 1971–1974.
[15] C. Li, J.H. Yum, S.J. Moon, A. Herrmann, F. Eickemeyer, M. Grätzel, M.K. Nazeeruddin, An improved perylene sensitizer for solar cell applications, ChemSusChem 1 (2008) 615–618.
[16] A.S. Lukas, Y. Zhao, S.E. Miller, M.R. Wasielewski, Biomimetic electron transfer using low energy excited states: a green perylene-based analogue of chlorophyll a, Journal of Physical Chemistry B 106 (2002) 1299–1306.
[17] F. Würthner, C. Thalacker, A. Sautter, W. Schärtl, W. Ibach, O. Hollricher, Hierarchical self-organization of perylene bisimide–melamine assemblies to fluorescent mesoscopic superstructures, Chemistry- A European Journal 6 (2000) 3871–3886.
[18] L.E. Sinks, B. Rybtchinski, M. Iimura, B.A. Jones, A.J. Goshe, X. Li, M.R. Wasielewski, Self-assembly of photofunctional cylindrical nanostructures based on perylene-3,4:9,10-bis(dicarboximide), Chemistry of Materials 17 (2005) 6295–6303.
[19] J. Feng, D. Wang, S. Wang, L. Zhang, X. Li, Synthesis and properties of novel perylenetetracarboxylic diimide derivatives fused with BODIPY units, Dyes and Pigments 89 (2011) 23–28.
[20] F. Würthner, V. Stepanenko, Z. Chen, N. Kocher, D. Stalke, Preparation and characterization of regioisomerically pure 1,7-disubstituted perylene bisimide dyes, Journal of Organic Chemistry 69 (2004) 7933–7939.
[21] F. Würthner, C. Thalacker, S. Diele, C. Tschierske, Fluorescent, J-type aggregates and thermotropic columnar mesophases of perylene bisimide dyes, Chemistry- A European Journal 7 (2001) 2245–2253.
[22] (a) J.M. Giaimo, A.V. Gusev, M.R. Wasielewski, Excited-state symmetry breaking in cofacial and linear dimers of a green perylenediimide chlorophyll analogue leading to ultrafast charge separation, Journal of the American Chemical Society 124 (2002) 8530–8531;
(b) B.T. Van der, R.T. Hayes, Y. Zhao, P.J. Bushard, E.A. Weiss, M.R. Wasielewski, Charge transport in photofunctional nanoparticles self-assembled from zinc 5 10,15,20-tetrakis-(perylenediimide)porphyrin building blocks, Journal of the American Chemical Society 124 (2002) 9582–9590.
[23] (a) C. Zafer, M. Kus, G. Turkmen, H. Dincalp, S. Demic, B. Kuban, New perylene derivative dyes for dye-sensitized solar cells, Solar Energy Materials and Solar Cells 91 (2007) 427–431;
(b) T. Dentani, K. Funabiki, J.Y. Jin, T. Yoshida, H. Minoura, M. Matsui, Application of 9-substituted 3 4-perylenedicarboxylic anhydrides as sensitizers for zinc oxide solar cell, Dyes and Pigments 72 (2007) 303–307.
[24] Y. Zhao, M.R. Wasielewski, 3,4:9,10-perylenebis(dicarboximide) chromophores that function as both electron donors and acceptors, Tetrahedron Letters 40 (1999) 7047–7050.
[25] M.K. Nazeeruddin, A. Kay, I. Rodicio, R. Humphry-Baker, E. Müller, P. Liska, N. Vlachopoulos, M. Grätzel, Conversion of light to electricity by cis-X_2Bis (2,2′-bipyridyl-4,4′-dicarboxylate)ruthenium(II) charge-transfer sensitizers (X = Cl⁻, Br⁻, I⁻, CN⁻, and SCN⁻) on nanocrystalline TiO_2 electrodes, Journal of the American Chemical Society 115 (1993) 6382–6390.

[26] S. Nakade, T. Kanzaki, W. Kubo, T. Kitamura, Y. Wada, S. Yanagida, Role of electrolytes on charge recombination in dye-sensitized TiO$_2$ solar cell (1): the case of solar cells using the I$^-$/I^{3-} redox couple, Journal of Physical Chemistry B 109 (2005) 3480–3487.

[27] S.Y. Huang, G. Schlichthörl, A.J. Nozik, M. Grätzel, A.J. Frank, Charge recombination in dye-sensitized nanocrystalline TiO$_2$ solar cells, Journal of Physical Chemistry B 101 (1997) 2576–2582.

[28] G. Boschloo, H. Lindström, E. Magnusson, A. Holmberg, A. Hagfeldt, Optimization of dye-sensitized solar cells prepared by compression method, Journal of Photochemistry and Photobiology A 148 (2002) 11–15.

[29] H. Kusama, Y. Konishi, H. Sugihara, H. Arakawa, Influence of alkeylpyridine additives in electrolyte solution on the performance of dye-sensitized solar cell, Solar Energy Materials and Solar Cells 80 (2003) 167–179.

[30] G. Boschloo, L. Haggman, A. Hagfeldt, Quantification of the effect of 4-tert-butylpyridine addition to I$^-$/I^{3-} redox electrolytes in dye-sensitized nanostructured TiO$_2$ solar cells, Journal of Physical Chemistry B 110 (2006) 13144–13150.

[31] W. Xu, S. Wang, Y. Weng, X. Li, Photoinduced electron and energy transfer in dyads of porphyrin dimer and perylene tetracarboxylic diimide, ChemPhysChem 9 (2008) 1409–1415.